Indian Journal of Pure & Applied Physics
Vol. 62, July 2024, pp. 538-546
DOI: 10.56042/ijpap.v62i7.9920

Design and Analysis of Asscher-shaped Two-element MIMO Antenna

B Tharini & A Kannammal
Department of ECE, PSG College of Technology, Coimbatore 641 004, India

Received 27 March 2024; accepted 24 May 2024

A compact two-element Asscher-shaped wideband MIMO antenna system is proposed in this communication. The Asscher-shaped MIMO system consists of a partial ground plane, an Asscher-shaped patch loaded with CSRR. The bandwidth of the antenna is from 2.5 to 6.4 GHz with a notch at 5.7 GHz which covers WLAN (4,6.2 GHz), WiMAX (4, 5.5 GHz), GSMA (3.5 to 4.2 GHz) and Mid band 5G (3.5 to 4.2 GHz). A decoupling structure enhances the isolation between its elements. The fabricated antenna accommodates 35.2 x67.5 x1.6 mm^3. The performance of Asscher shaped MIMO antenna is assessed using the S-parameters, radiation pattern, ECC, DG, TARC, MEG, and CCL. The results from simulation and measurement are validated and both accord well. The antenna design involves simple geometry with no intricate process in fabrication.

Keywords: Diversity metrics; Asscher shape; MIMO; Isolation

1 Introduction

With the increase in the number of users and rapid evolution of wireless technology, an increment in bandwidth is required. The backbone of the current requirement is the MIMO systems. Traditional solutions involve bigger size, low gain, and reduced bandwidth. To overcome the above limitations MIMO antennas are preferred. The reported MIMO performance parameters include ECC, DG, MEG, TARC, and CCL. Various MIMO configurations were reported in the literature.

Various methods have been developed to maximize bandwidth, gain, and minimize coupling between the radiating elements. For instance, in the case of isolation enhancement, a cross-shaped stub was placed between the radiating elements[1]. To lower the coupling, the edge-to-edge separation between the radiating elements is widened[2]. Ground-based CSRR was developed for reduced coupling, bandwidth increase, and antenna size miniaturization[3]. L-shaped feed and circular quadrants obtain the wideband response[4]. Meander lines with partial ground in the antenna design reduce coupling. L-shaped slots were added to the patch for bandwidth enhancement[5]. To increase bandwidth, reverse L-shaped and line-shaped slots were added to the patch and parasitic elements on the ground plane[6]. The Two rectangular notches form the radiating patch joined to make a T-shaped notch and Clover-leaf arm-shaped antenna with superstrate for wideband characteristics[7,8]. In[9] a MIMO system with a hexagonal loop superstrate layer has a bandwidth of 0.37 GHz and an isolation of 24 dB. Defected annular rings, slots, and an isolating structure were employed for the enhancement of bandwidth and gain[10]. A defected complementary open loop resonator was introduced for triple band application[11]. The parasitic decoupling structure in the MIMO antenna improves isolation[12]. The impedance bandwidth was enhanced by the MIMO technique[13]. To increase isolation between the antenna elements, meander lines, and split ring resonators were used[14]. The MIMO antenna in[15] was designed to cover a bandwidth of 2.15 GHz. The frequency-agile antenna was designed with rectangular CSRR decoupled elements to weaken the coupling between the elements[16]. To lower the coupling of multi-slot isolating elements, meander lines, triangular split ring resonators, circular split ring resonators, U-shaped slots, superstrate layers and parasitic structure, the position of patches and orthogonally placed separate monopole ground can be considered[17-20]. Four L-shaped patch elements were placed beside one another with a common ground plane and to reduce the inter-element coupling parasitic structures were used[21]. To provide good isolation, T-slots, and Pi-shaped slots were integrated in radiating patches of the MIMO antenna, which was constructed using a labyrinth split ring resonator[22-24].

*Corresponding authors:
(E-mail: tharinibm@gmail.com; aks.ece@psgtech.ac.in)

The following are some advantages of the suggested Asscher-shaped MIMO antenna over the previously mentioned antenna,

- The Asscher-shaped MIMO antenna is designed in such a manner that it achieves wider bandwidth and high isolation, MIMO attributes like ECC, DG, CCL, TARC, and MEG are in an acceptable range.
- To overcome the narrow bandwidth in the aforementioned papers, the bevel cut-corner concept is introduced to achieve wider bandwidth.
- The proposed antenna is easy to fabricate since it has simple geometry with low-cost dielectric material FR-4.

2 Methodology

The design of a two-element Asscher-shaped MIMO antenna starts with a single square patch antenna and is later transformed into a two-element MIMO antenna separated by a decoupling element.

2.1 Design Configuration

The suggested layout of the two-element MIMO antenna is depicted below in Fig. 1(a & b). Two Asscher-shaped patches, a decoupling element, and a common partial ground planemake up the Asscher-shaped MIMO antenna. The dielectric material used here is the FR 4 substrate (loss tangent=0.02, relative permittivity=4.4, thickness=1.6mm). The ANSYS HFSS software is employed for simulation. The prototype of the suggested Asscher-shaped MIMO antenna is shown in Fig. 2 (a & b).

2.2 Design flow of the proposed antenna

The evolution of the proposed two-element antenna starts from the design of antenna-1 as depicted in Fig. 3(a) which is square (20 mm x 20 mm)[25]. The antenna-1 resonates from 2.88 GHz to 5.28 GHz. Then as shown in Fig. 3(b) the square-shaped patch corners are etched to form an Asscher-shaped radiating patch designated as antenna-2 that on excitation resonates from 2.8 GHz to 5.57 GHz. The truncated corner concept is introduced to induce discontinuity in the wave flow and increasing the reflections will eventually improve the bandwidth[26]. Now antenna-3 as depicted in Fig. 3(c) is loaded with CSRR, due to which the antenna-3 exhibits a stop band at 5.7 GHz. The stop band response is due to the addition of CSRR and it is feasible to control the resonance characteristics of the antenna and as a result, additional resonance is created by the

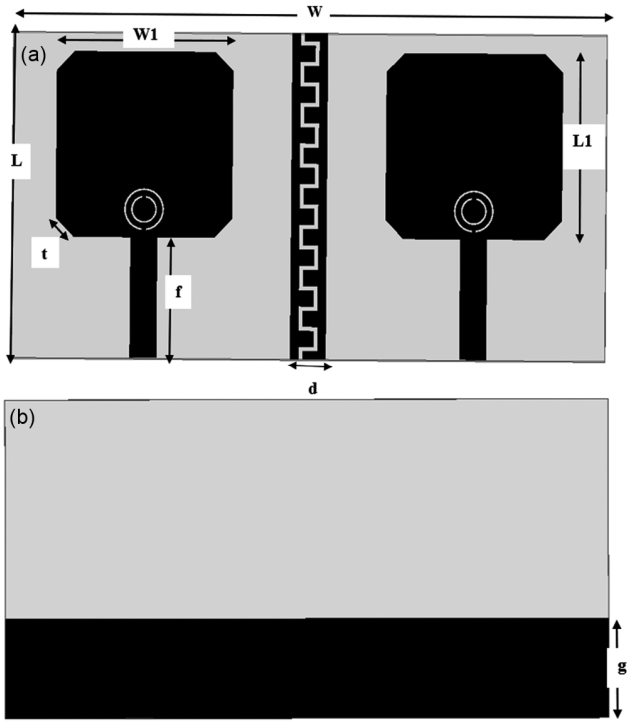

Fig. 1 — Layout of the Asscher-shaped MIMO antenna (a) Top view (b) Bottom view Dimensions: W=67.5 mm, L=35.2 mm, W1=20 mm, t=2.82 mm, f=13 mm, d=4mm, L1=20 mm, g=11 mm

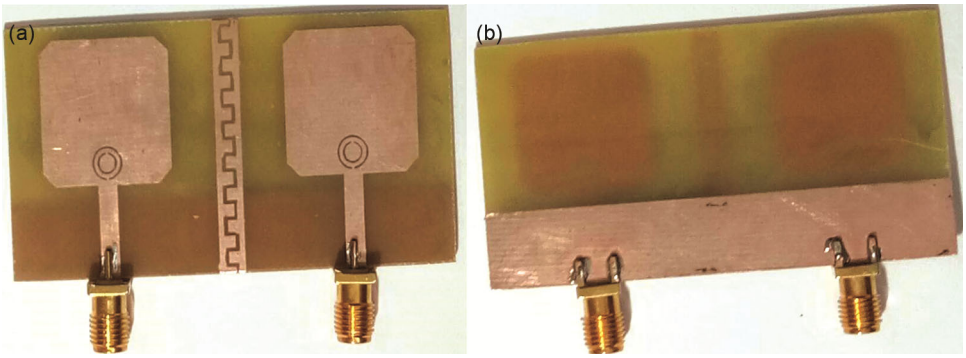

Fig. 2 — Fabricated Asscher-shaped MIMO antenna (a) Top view (b) Bottom view

strategical placement of the same CSRR structure in antenna-3[29].

The design of MIMO antenna aims to enhance their characteristic concerning bandwidth, size miniaturization, and isolation. The Asscher-shaped two-element MIMO antenna with common partial ground is depicted in Fig. 3(d) and is referred to as antenna-4. Now a decoupling structure is inserted between the two Asscher-shaped elements as shown in Fig. 3(e) referred to as antenna-5 to lower the mutual coupling. The decoupling structure not only reduces the coupling but also increases the impedance match between the antenna components. This alteration in impedance matching impacts the resonant frequency thereby aligning it better with the intended operating frequency. The decoupling element has increased the level of isolation between the patches and there is a significant change in the reflection coefficient. The plot of the reflection coefficient and mutual coupling of Asscher shaped the MIMO design is depicted below in Fig. 4(a-c).

From Fig. 4(b) from the simulated S_{11} plot of antenna-5, the antenna exhibits resonance from 2.5 GHz to 6.1 GHz except at 5.7 GHz due to the stop band characteristic of CSRR. From Fig. 4(c), it is evident that the decoupling element reduces the coupling which is less than -18 dB.

2.3 CSRR

Metamaterials are artificial composite materials that are not readily available in nature. The CSRR used in this design is a single negative metamaterial *i.e.*, Mu-Negative Metamaterial. Split ring resonators are the most widely used MNG material[30,32]. To explore the performance of CSRR, the CSRR is placed on top of the FR-4 substrate as depicted in Fig. 5. In the above setup, the Perfect Magnetic Field is assigned to the top and bottom of the setup whereas

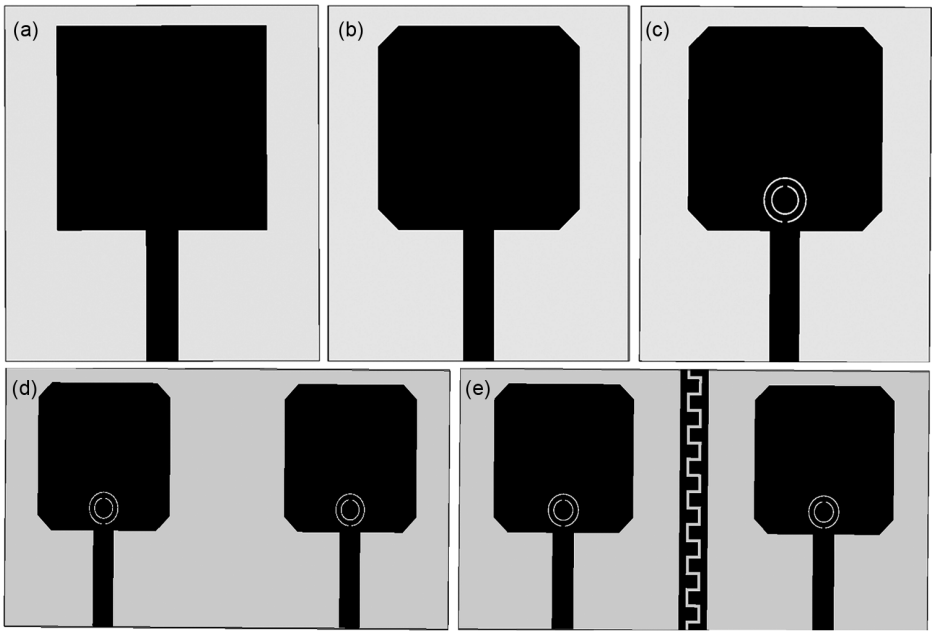

Fig. 3 — Design flow of the antenna (a) antenna-1 (b) antenna-2 (c) antenna-3 (d) antenna-4 and (e) antenna-5

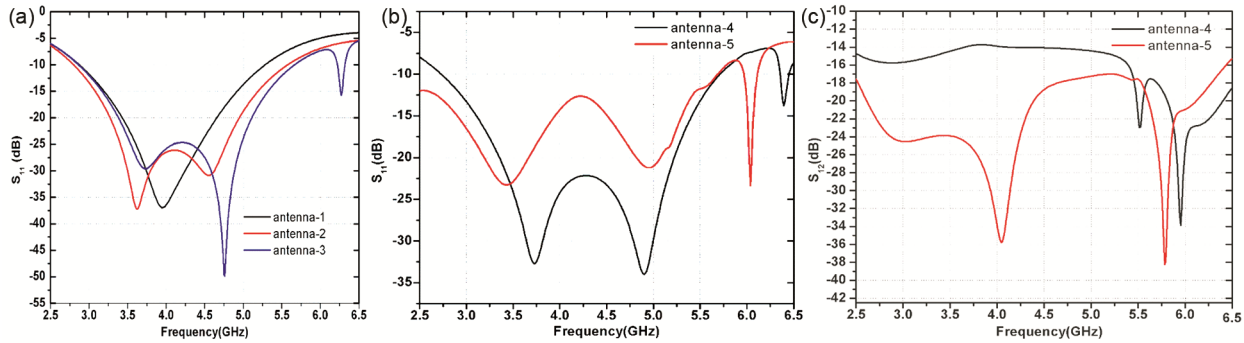

Fig. 4 — (a) Simulated S_{11} plots of antenna-1,2,3 (b) Simulated S_{11} plots of antenna-4,5 (c) Simulated S_{12} plots of antenna-4,5.

the setup's front and rear sides are designated for the Perfect Electric Field and the excitation signal is given on the other two sides. When the CSRR structure is excited with an EM wave, the scattering parameters S_{11} and S_{21}, exhibits stop band characteristics at 5.7 GHz as shown in Fig. 6(a)

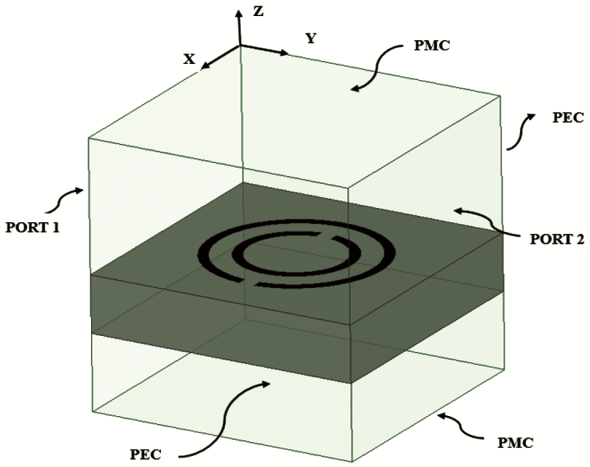

Fig. 5 — Setup of CSRR

3 Results and Discussion

The above setup of CSRR is a single negative metamaterial. The permeability values of the CSRR structure is extracted from MATLAB 2016Ra and the permeability is plotted as shown below in Fig. 6(b). From Fig. 6(b) the negative permeability indicates that the CSRR is a single negative metamaterial. From both the scattering parameter plot and the permeability plot negative characteristic is at 5.7 GHz, thereby exhibiting the stop band.

The Vector Network Analyser Agilent N5247A is used to test the fabricated MIMO antenna as shown in Fig. 7 (a & b) below. The differences in simulation and measured results are due to the fabrication tolerances.

The plot of the reflection coefficient is depicted in Fig. 8 In the case of simulation, the resonance of Asscher shaped two-element MIMO antenna is from 2.5 GHz to 6.1 GHz with a notch at 5.7 GHz whereas in the case of measurement, the fabricated antenna's resonance is from 2.5 GHz to 6.4 GHz with a notch at

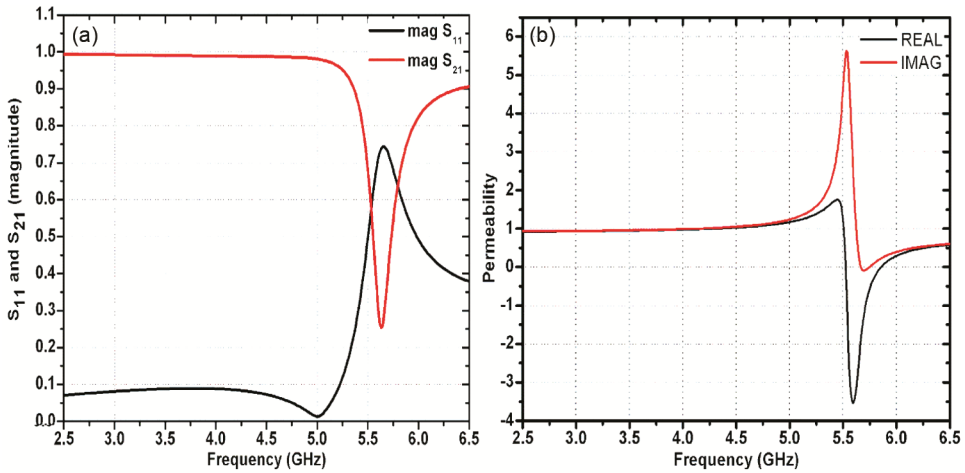

Fig. 6 — (a) Response of S_{11} and S_{21} (b) Permeability responseof CSRR

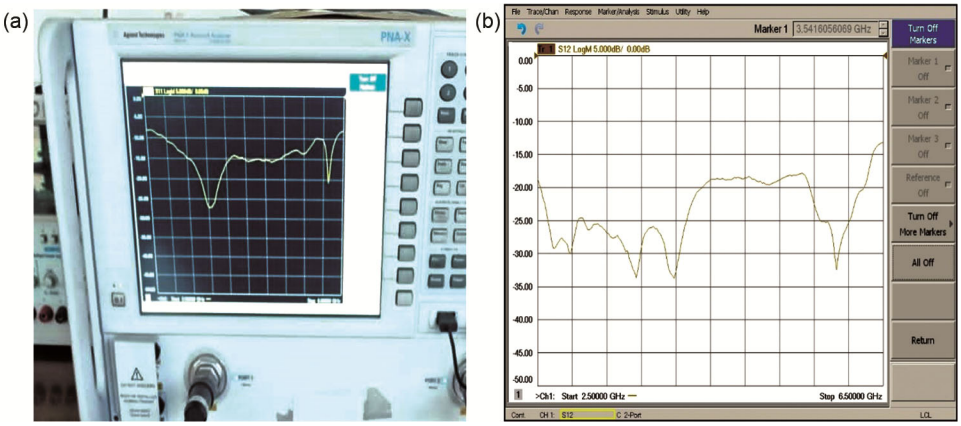

Fig. 7 — (a) Measured S11 plot (b) Measured S12 plot

5.7 GHz. Fig. 9 depicts the mutual coupling plot in the case of simulation and measurement, the value of coupling is below -18 dB for the resonating frequencies.

3.2 Attributes of the MIMO antenna

The far-field characteristics of the two-element Asscher-shaped MIMO antenna are analyzed with the help of an anechoic chamber as illustrated in Fig. 10

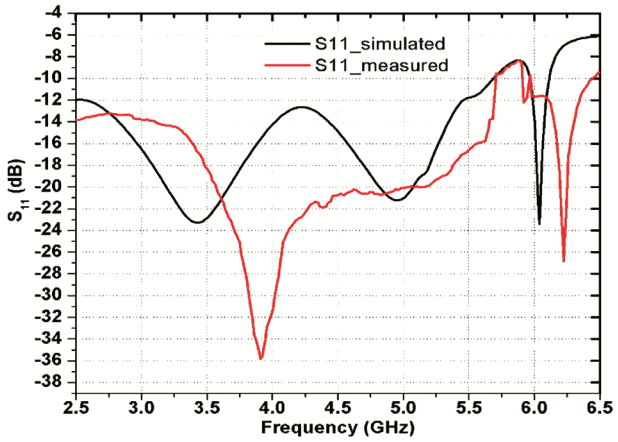

Fig 8 — Simulated and measured S_{11} plot

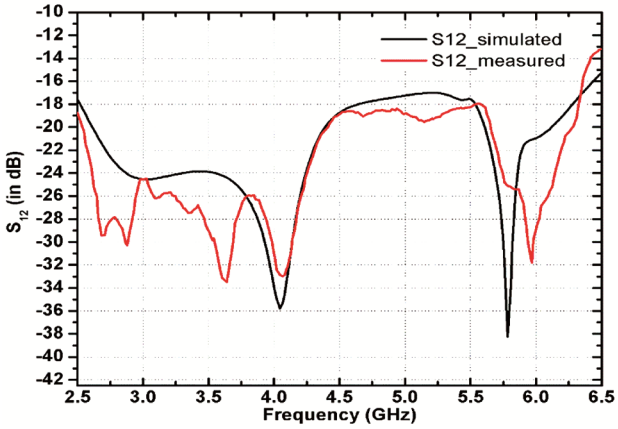

Fig. 9 — Simulated and measured S_{12} plot

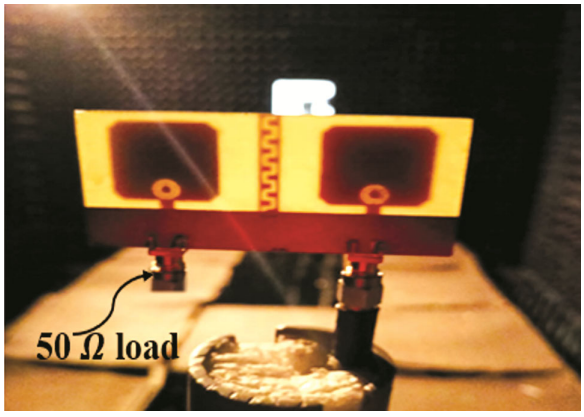

Fig 10 — Asscher-shaped MIMO antenna in an anechoic chamber

The fabricated MIMO antenna behaves as an antenna under test and in the place of the reference antenna horn antenna is placed at a reasonable distance based on the far field condition. The plot of gain for the Asscher-shaped MIMO antenna is depicted in Fig. 11.

Gain is maximum at 5 GHz. The CSRR functions as a selective filter, attenuating specific frequencies while other frequencies are permitted. At the notch frequency, CSRR acts as a selective filter suppressing only certain frequencies, leading to improved reasonable gain at the notch band. Whereas at lower frequencies CSRR interacts with the antenna resonance leading to a mismatch between CSRR resonant frequency and antenna's operating frequency introduces reactance leading to higher insertion loss, reducing gain at lower frequencies. From the above figure, the gain is reduced in the lower part and the variation in gain is from 2.36 dBi to 4.96 dBi in the case of simulation and measured case, the variation in gain is from 2.02 dBi to 3.71 dBi.

The 2-D radiation pattern in E-plane and H-plane are depicted at 3.5 GHz and 6 GHz as shown in Fig. 12 (a & b). The E and H plane pattern is nearly omni directional and dumbbell shaped and the distortion in the pattern is due to the decoupling structure placed between the radiating patches. In practical antenna manufacturing, there are always tolerances and variations in the dimensions, materials, and assembly process. These discrepancies can lead to variations in the antenna performance compared to the idealized model used in the simulation.

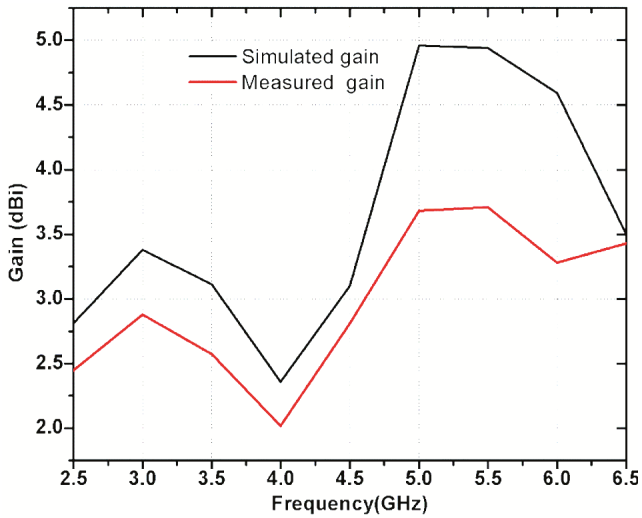

Fig. 11 — Gain plotof the Asscher-shaped MIMO antenna with the decoupling element

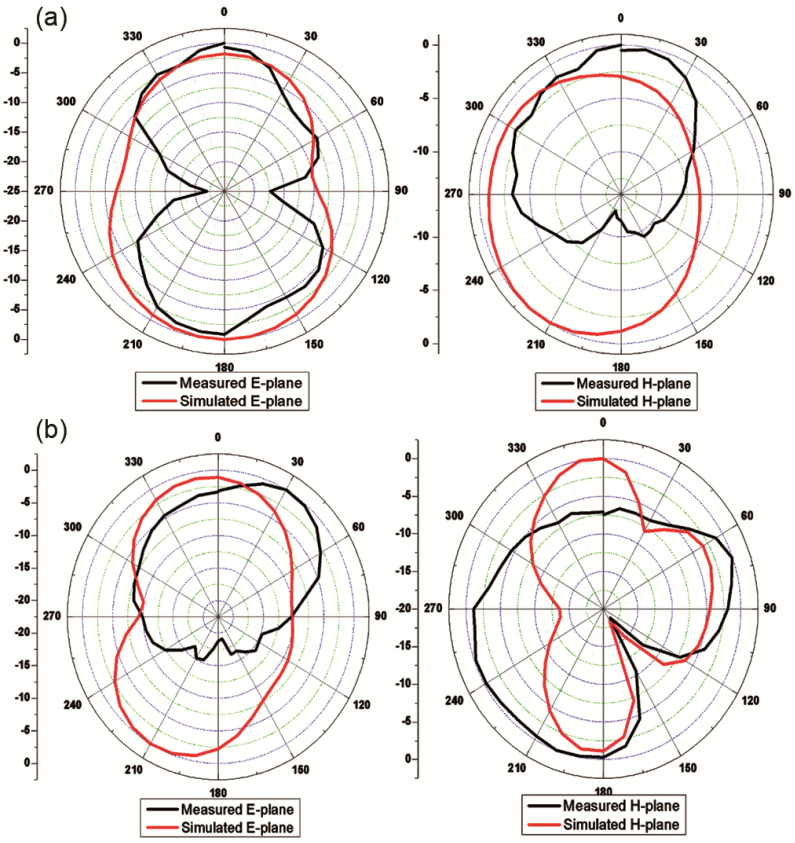

Fig. 12 — Radiation plots (a) 3.5 GHz and (b) 6 GHz

3.1 Diversity attributes of the MIMO antenna

The suggested two-element Asscher-shaped MIMO antenna is examined for several characteristics, including Envelope Correlation Coefficient (ECC), Diversity Gain (DG), Total Active Reflection Coefficient (TARC), Mean Effective Gain (MEG), and Channel Capacity Loss (CCL).

(a) Envelope Correlation Coefficient (ECC)

To examine the coupling of the MIMO antenna ECC is numerically calculated. To calculate ECC, S-parameter and field pattern are used[3,5,27,28] as per Eqs. (1) & (2).

$$ECC = \frac{|S_{11}^{*}S_{12}+S_{11}^{*}S_{22}|}{(1-|S_{11}|^{2}-|S_{21}|^{2})(1-|S_{22}|^{2}-|S_{12}|^{2})} \quad ...(1)$$

$$ECC = \frac{\left|\iint F_{1(\theta,\varphi)}\cdot F_{2(\theta,\varphi)}\, d\Omega\right|^{2}}{\iint |F_{1(\theta,\varphi)}|^{2}\, d\Omega \cdot \iint |F_{2(\theta,\varphi)}|^{2}\, d\Omega} \quad ...(2)$$

$F_{i(\theta,\varphi)}$=Field pattern of antenna elements with respect to θ and φ

$\Omega = solid\ state\ angle$, and

• = Hermitian product

Ideally, the value of ECC should be zero for the MIMO elements to have zero correlation. The measured and simulated ECC plot is depicted in Fig. 13.

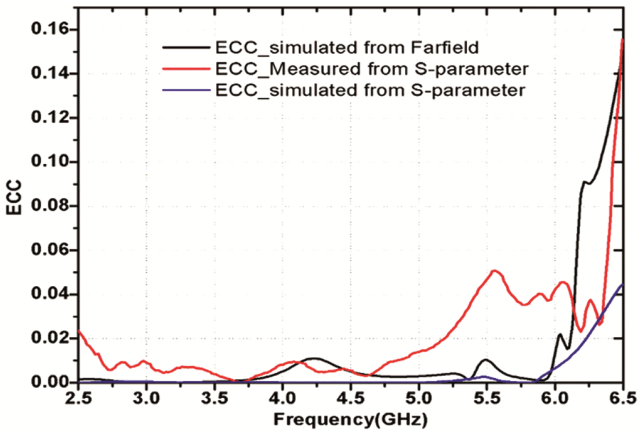

Fig. 13 — ECC plot of the Asscher-shaped MIMO antenna

From Fig. 13, it is clear that ECC is within the acceptable range ie., ECC should be less than 0.5. Here the obtained value of ECC is below 0.16 for the resonating frequencies.

(b) Diversity Gain (DG)

To characterize MIMO, diversity gain is taken into account. Eq. (3) provides the relationship between ECC and DG[5,31].

$$DG = 10\sqrt{1-(ECC)^2} \quad \ldots(3)$$

Ideally, the value of DG should be >9.5 dB. From Fig. 14, it is clear that DG is in the acceptable range greater than 9.9 dB.

(c) Total Active Reflection Coefficient (TARC)

For any N-port network, TARC gives the relationship between the incident power and outgoing power. TARC is calculated from expression (4) for different phase angles with a step size of 30 degree[3,5,31].

$$TARC = \frac{\sqrt{\sum_{m=1}^{n}|S_{m1}+\sum_{p=2}^{n}e^{m\theta_{p-1}}|^2}}{\sqrt{n}} \quad \ldots(4)$$

TARC should ideally have a value of less than -10 dB. Fig. 15 makes it obvious that computed TARC values are less than -10 dB for all the resonating frequencies from 2.5 GHz to 6.4 GHz in case of higher angles.

(d) Mean Effective Gain (MEG)

To analyze the MIMO system MEG plays a key role. In the fading environment MEGis the mean received power[3,10]. MEG-1 and MEG-2 are calculated using Eqs (5) & (6). MEG is extracted using Eq. (7)

$$MEG_P = 0.5\left[1-|S_{pp}|^2-|S_{pq}|^2\right] \quad \ldots(5)$$

$$MEG_q = 0.5\left[1-|S_{pq}|^2-|S_{qq}|^2\right] \quad \ldots(6)$$

$$\text{MEG} = \left|MEG_P - MEG_q\right| \quad \ldots(7)$$

A MIMO system is said to operate better only if the ratio of MEG-1 and MEG-2 is less than 3 dB. Regarding the suggested Asscher-shaped MIMO antenna MEG is in the range of 1.1 dB which is depicted in Fig. 16.

(e) Channel Capacity Loss (CCL)

For the analysis of the MIMO system, CCL is one of the key parameters to be examined. The CCL denotes the maximum distance at which no loss will occur during transmission. The ideal value of CCL should be less than 0.5[12,28,31]. CCL is calculated using the expression (8), (9), (10), (11), (12), and (13).

$$CCL = -log_2|C^R| \quad \ldots(8)$$

$$C^R = \begin{bmatrix} C_{11} & C_{12} \\ C_{21} & C_{22} \end{bmatrix} \quad \ldots(9)$$

$$C_{11} = 1-(|S_{11}|^2+|S_{12}|^2) \quad \ldots(10)$$

$$C_{12} = -(S_{11}^*S_{12}+S_{21}^*S_{22}) \quad \ldots(11)$$

$$C_{21} = 1-(S_{22}^*S_{21}+S_{21}^*S_{22}) \quad \ldots(12)$$

$$C_{22} = 1-(|S_{22}|^2+|S_{21}|^2) \quad \ldots(13)$$

From Fig. 17, it is observed that the plot of CCL is less than 0.5 bits/sec/Hz which indicates that the loss during transmission is negligible.

Table 1 compares the results of the proposed work with previous other works

Finally, from Table 1 a comparison of the suggested antenna's characteristics with those other

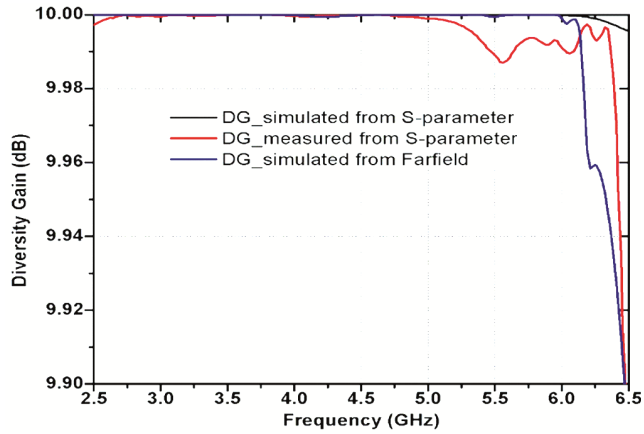

Fig. 14 — DG plot of the Asscher-shaped MIMO antenna

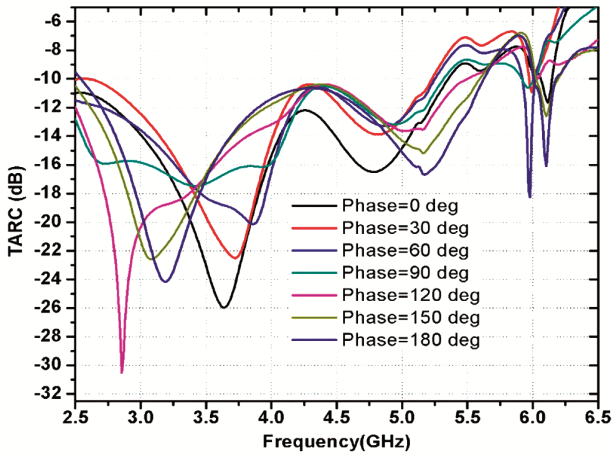

Fig. 15 — TARC plot of the Asscher-shaped MIMO antenna

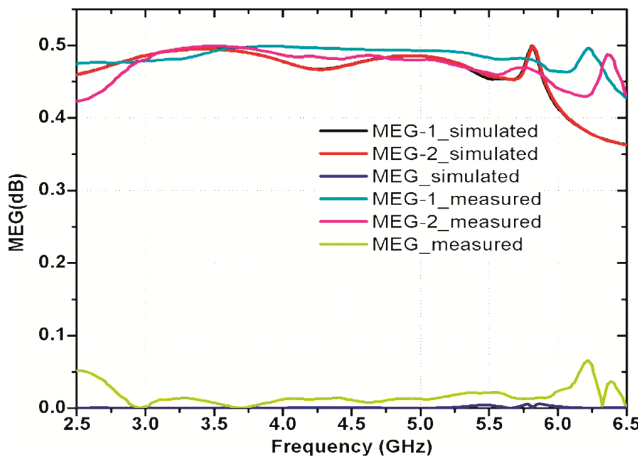

Fig 16 — MEG plot of the Asscher-shaped MIMO antenna

Table 1 — Comparison of Asscher-shaped MIMO with previous works

Ref.	Operating frequency (GHz)	Dimension in mm^2	Gain (dBi)	No. of elements	Isolation (dB)	ECC
[1]	2.3-2.7	66 x 66	3.7	4	-17	0.04
[3]	2.85 -3.04 5.61 – 5.8	106.6 x106.6	3.8 4.32	4	-24	0.01
[5]	4.1 -6.1 1.5 -3.8	97 x 110	4	4	-25	0.1
[6]	2.3 -3.1 4.9-6.1	102 x 52	5	8	-15	0.5
[11]	2.22-2.54 3.14-3.9 5.3-5.7	95 x 21	3.2	2	-34	0.01
[16]	1.8 2.4 3.5	66 X 60	1.95	4	-28	<0.5
[18]	5.65-6.06	70 x 60	3.73	4	-21	<0.003
[19]	5.15 – 5.85	39 x 30	2.8	4	-20	-
[20]	3.28-3.624.78-5.04	38 x 38	3.4	4	-17.5 -19.5	<0.035
[22]	2.33-2.48	24.3 x 42.9	-	2	-55	0.05
[23]	2.4 5.2 5.8	52 x 77.5	3.6 3.75	2	-20	-
[24]	5.2	45 x 21	5.8	2	-20	0.04
[27]	3.4-3.625 3.9-4.525	170 x 80	6.5	4	-20.1	<0.3
[28]	2.8052-3.788 5.3818-6.3834	47.4 x 31.7	5	2	-25	<0.012
Proposed work	2.5-6.42	35.2 x 67.5	S=4.96 M=3.71	2	<-18	<0.01

(S=Simulated, M= Measured)

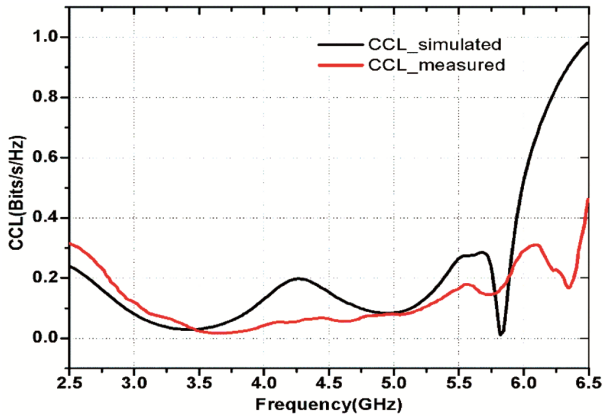

Fig 17 — CCL plot of the Asscher-shaped MIMO antenna

MIMO designs is made to emphasize its badvantages. The reported MIMO antenna[3,5,16,22] provides slightly lower isolation than the suggested antenna, whereas the foresaid antenna operates for minimal bandwidth. The other reported MIMO configurations have larger foot print than the suggested antenna. On the whole, the suggested Asscher shaped MIMO antenna has a compact size with wider bandwidth than the foresaid antenna's with better MIMO attributes.

4 Conclusion

This paper presented a two-element Asscher shaped MIMO antenna using CSRR to achieve wideband characteristic with stop band at 5.7 GHz. The Asscher-shaped MIMO antenna is evaluated for various parameters. The decoupling element between elements of the antenna provides better isolation of about less than -18 dB. The fabricated Asscher shaped MIMO antenna prototype was validated and the measured and simulated results agree with each other. From the simulated and measured MIMO attributes, it can be concluded that the MIMO system has ECC<0.15, DG>9.9 dB, MEG<1.1 dB, TARC <-10 dB and CCL <0.5 Bits/sec/Hz. Its wideband of operation ranging from 2.5 GHz to 6.4 GHz makes it a good contender for applications like (4/6.2 GHz)

WLAN, (4/5.5 GHz) WiMAX, GSMA (3.5 to 4.2 GHz) and Mid-band 5G (3.5 to 4.2 GHz) applications.

References

1 Yussuf A A & Paker S, *AEU-Int J Electron Commun*, 111 (2019) 152893.
2 Saadh A M, Ashwath K, Ramaswamy P, Ali T & Anguera J, *AEU-Int J Electron Commun*, 123 (2020) 153316.
3 Murtala A B, Mohamad K A I, Farid Z, Adamu Y I, Kabiru I J, Mohd F M & Irene K, *Int J Electron Commun*, 136 (2021) 1.
4 Raj R K, Sharma V K, Saxena A U, Choudhary H & Joshi P, *Indian J Eng Mater Sci (IJEMS)*, 30 (2023) 603.
5 Roy S, Ghosh S, Pattanayak S S & Chakarborty U, *Int J RF Microwave Comput-Aided Eng*, 30 (2020) e22292.
6 Roy S, Ghosh S & Chakarborty U, *Int J RF Microwave Comput-Aided Eng*, 29 (2019). e21749.
7 Verma R K, *Int J Numer Model Electron Networks, Dev Fields*, 37 (2024) e3178.
8 Hakim B, Kumar A, Yousaf J, Sheikh M, Rmili H & Mittra R, *Int J Numer Model Electron Networks, Dev Fields*, 33 (2020) e2705.
9 Mark R, Rajak N, Mandal K & Das S, *AEU-Int J Electron Commun*, 100 (2019) 144.
10 Yadav V, Yadav R S, Yadav P, Mishra B & Kumar A, *AEU-Int J Electron Commun*, 162 (2023) 154576.
11 Ekrami H & Jam S, *AEU-Int J Electron Commun*, 96 (2018) 219.
12 Ayinala K D & Sahu P K, *AEU-Int J Electron Commun*, 142 (2021) 154013.
13 Ghadeer S H, Rahim S K A, Alibakhshikenari M, Virdee B S, Elwi T A, Iqbal A & Al-Hasan M, *AEU-Int J Electron Commun*, 159 (2023) 154480.
14 Nagendra R & Swarnalatha S, *ICT Express*, 8 (2022) 235.
15 Mohammad S A W, Khangarot S, Sravan B V, Aluru N, Ramaswamy P, Ali T & Pai M M, *Int J Commun Syst*, 33 (2020) e4506.
16 Singh G, Kumar S, Kanaujia B K & Pandey V K, *AEU-Int J Electron Commun*, 146 (2022) 154118.
17 Ameen M, Ahmad O & Chaudhary R K, *AEU-Int J Electron Commun*, 124 (2020) 153336.
18 Mark R, Rajak N, Mandal K & Das S, *Radioengineering*, 28 (2019) 689.
19 Cheng Y, Liu H, Sheng B Q & Zhu L, *Microwave Opt Technol Lett*, 62 (2020) 2930.
20 Sun Y, Pan T, Wang Q & Huang F, *Progress Electromagn Res Lett*, 105 (2022).
21 Azari-Nasab T, Ghobadi C H, Azarm B & Majidzadeh M, *Int J Microwave Wireless Technol*, 12 (2020) 259.
22 Torabi Y, Bahri A & Sharifi A R, *IETE J Res*, 62 (2016) 106.
23 Bharathi A & Gosula R S R, *IETE J Res*, 69 (2023) 1466.
24 Sharma V, Goel A, Upadhayay M D & Singh A V, *IETE J Res*, 69 (2023) 1613.
25 Balanis C A, *Antenna theory: analysis and design*, John wiley & sons, (2016).
26 Baudha S & Kumar D, *Microwave Opt Technol Lett*, 57 (2015) 845.
27 Jha P, Kumar A, De A & Jain R K, *Progress Electromagn Res Lett*, 101 (2021) 35.
28 Mood Y & Pandeeswari R, *Wireless Personal Commun* 130 (2023) 1277.
29 Shobana M, *Alex Eng J*, 77 (2023) 351.
30 Li J, Zhao J B, Liang J J, Zhong L L & Hong J S, *Microwave J*, 61 (2018).
31 Keshri P K, Sahu S K & Chandel R, *IETE J Res*, 69 (2023) 6709.
32 Kaur P, Bansal S & Kumar N, *J Eng Appl Sci*, 69 (2022) 47.